Electronic Supplementary Information

Porous SnO_2 Nanosheets for Room Temperature Ammonia Sensing in Extreme Humidity

*Mohit Verma[1], Gaurav Bahuguna[1], Sukhwinder Singh[1], Ankita Kumari[2], Dibyajyoti Ghosh[2,3] Hossam Haick[4], and Ritu Gupta[1,2]**

[1]Advanced Materials and Devices Laboratory, Department of Chemistry, Indian Institute of Technology Jodhpur, Jodhpur, Rajasthan-342037, India
[2]Department of Chemistry, Indian Institute of Technology, Delhi, Hauz Khas, New Delhi 110016, India
[3]Department of Materials Science and Engineering, Indian Institute of Technology, Delhi, Hauz Khas, New Delhi 110016, India
[4]Department of Chemical Engineering and Russell Berrie Nanotechnology Institute, Technion – Israel Institute of Technology, Haifa 3200003, Israel

*Corresponding Author: Prof. Ritu Gupta (ritugupta@iitd.ac.in)

Table of Contents:

	and pore volume.
Figure S8:	XPS survey spectrum of SnO_2 nanosheets synthesised at different pH conditions.
Figure S9:	High resolution Sn3d and C1s XPS spectrum of SnO_2 nanosheets synthesised at different pH conditions.
Table S4:	High-resolution XPS peak positions of SnO_2 nanosheets synthesized at different pH conditions.
Table S5:	Oxygen defects concentration of SnO_2 nanosheets synthesized at different pH conditions.
Figure S10:	Schematic of the custom gas sensing setup for dynamic experiments.
Figure S11:	Variation in baseline current of SNS-14 at varying humidity.
Figure S12:	Sensing transients of SNS-14 towards different relative humidity (70-90%RH).
Figure S13:	SNS-14 response toward 100 ppm ammonia at a varying relative humidity of 60-90% at room temperature.
Figure S14:	Long-term stability of SNS-14 sensor towards 100 ppm ammonia under humid circumstances (90% RH).
Figure S15:	SNS-14 sensor (a) ammonia detecting transients for five cycles and (b) corresponding response value toward 100 ppm NH_3 at 25°C and 90% RH, demonstrating repeatability.
Figure S16:	The current response of the SNS-14 toward a healthy person's breath and the simulated diseased breath containing 1 ppm NH_3.
Figure S17:	The 3D plots of the charge density difference $\Delta\rho(r)$ of the (a) H_2O and (b) NH_3 molecules on the (110) surface of SnO_2. Electron depletion and accumulation are depicted by blue and green areas, respectively. The isosurfaces are plotted as values of $\pm 0.002\ \lvert e \rvert\ Å^{-3}$. These depict that the NH_3 molecule donates charge to the surface much more significantly than the H_2O molecule.

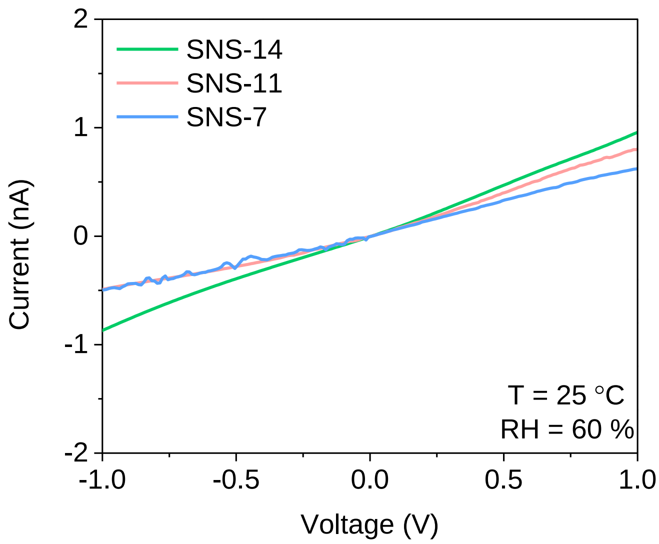

Figure S1: I-V characteristics of sensors based on SnO_2 nanosheets.

Table S1: A literature survey of gas/VOC sensors fabricated using SnO_2 nanosheets.

Sensing gas/VOC	Temp (°C)	Response (a, b, c) (conc. ppm)	$T_{res.}$ (s)	T_{rev} (s)	LOD (ppm)	RH (%)	Ref.
Ammonia	25	106.5^{a} (100)	8	55	0.000064	70%	This work
H_2	300	7.5^{b} (500)	6	12	NA	NA	1
CH_4	300	1.3^{b} (500)	18	28	NA		
HCHO	120	57^{b} (100)	1.1	1.5	NA	NA	2
Ethylene glycol	220	395^{b} (400)	65	72	1.37	NA	3
Acetic acid	340	672^{b} (500)	11	6	NA	NA	4
CO	300	60^{b} (100)	8	15	NA	30%	5
Ethanol	165	50.1^{b} (50)	29	136	NA	NA	6
Ethanol	275	33^{b} (100)	11	125	NA	NA	7
Ethanol	300	39.6^{b} (6)	1	9	NA	NA	8
Ethanol	250	73.3^{b} (100)	NA	NA	NA	NA	9
CO	300	-(100)	1	3	NA		
Ethanol	275	56.2^{b} (100)	NA	NA	NA	NA	10
Ethanol	350	48.37^{b} (100)	8	NA	NA	NA	11

^{a} $\Delta R/R_a$ (%) or $\Delta G/G_a$ (%) or $\Delta I/I_a$ (%)},

[b]R_a/R_g or G_a/G_g or I_a/I_g},
[c]$\Delta R/R_a$ or $\Delta G/G$ a or $\Delta I/I_a$}

NA: Not Available

$R_a/I_a/G_a$: resistance/current/conductance of material in the presence of air

$R_g/I_g/G_g$: resistance/current/conductance of material in the presence of gas

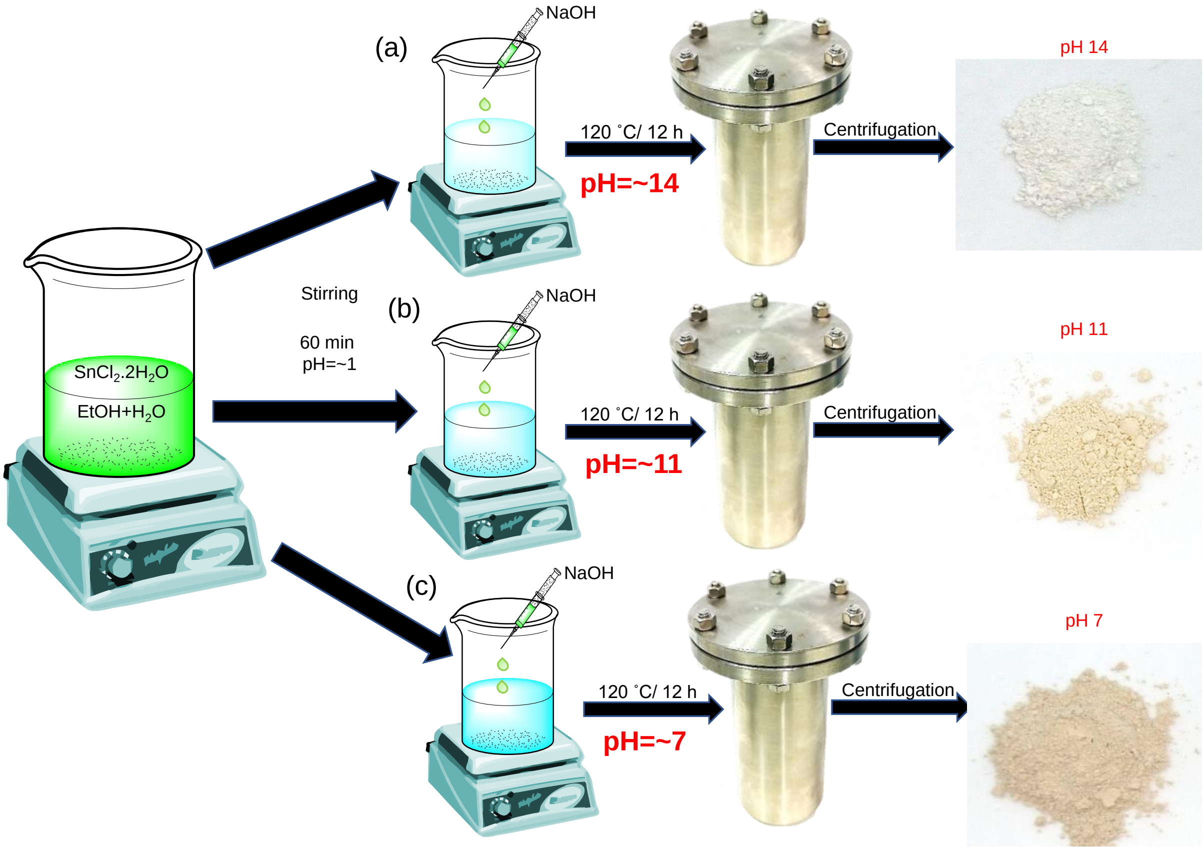

Figure S2: Schematic depiction of procedure adopted for SnO_2 nanosheet synthesis at different pH conditions of precursor solution before solvothermal reaction.

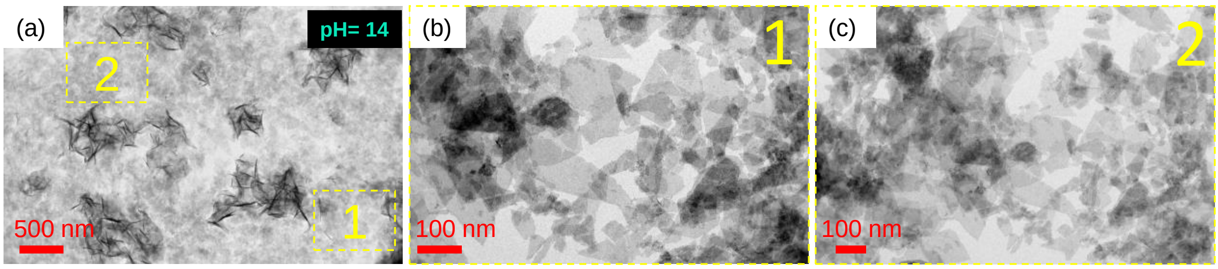

Figure S3: (a) Low magnification TEM images of SnO_2 nanosheets synthesized at pH 14 conditions to show uniformly dispersed nanosheets.

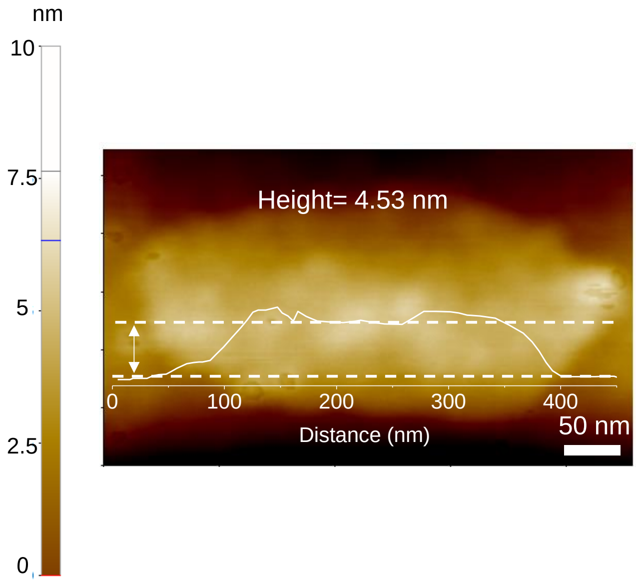

Figure S4: AFM image and height profile analysis of SnO_2 nanosheets.

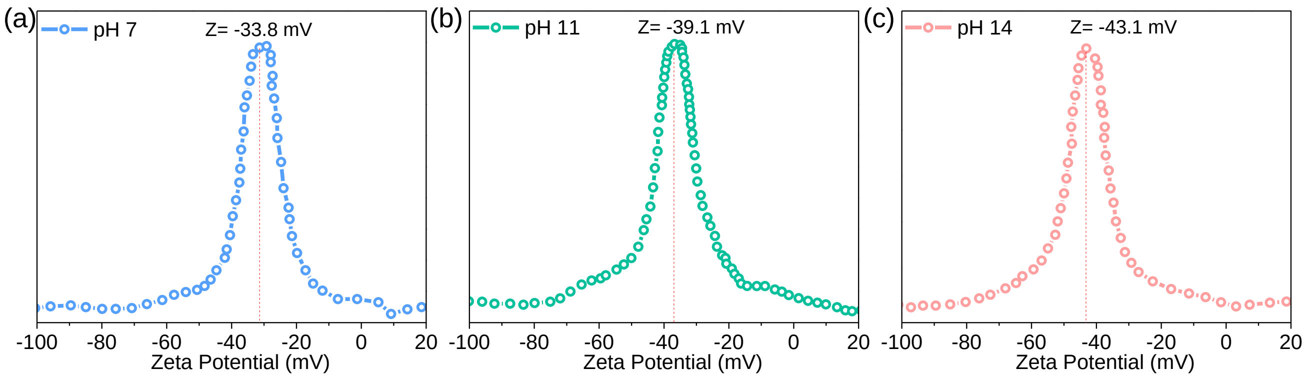

Figure S5: (a-c) Zeta potential of SnO_2 nanosheets synthesized at different pH conditions.

The stability of SnO_2 nanosheets at pH 14 is much higher than at pH 11 and pH 7.

Table S2: Crystallite size calculation from XRD data using Scherrer formula.

Sample	(110)	(101)	(200)	(211)	Average Crystallite Size (nm)
pH 7	3.95	3.90	2.30	3.62	3.44
pH 11	4.17	3.92	2.92	3.79	3.70
pH 14	7.77	6.35	5.55	4.82	6.12

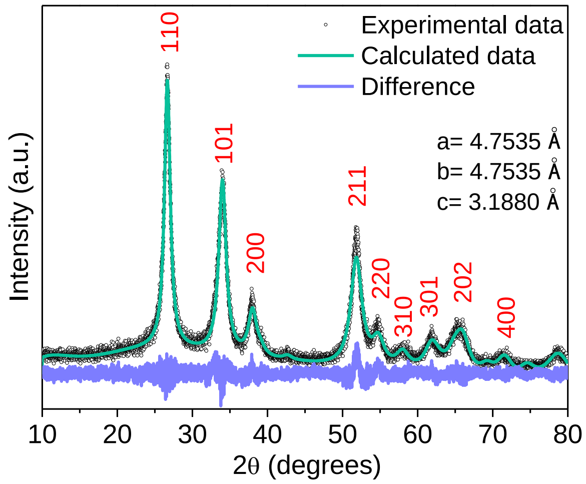

Figure S6: Rietveld refinement of the X-ray diffraction pattern of SnO_2 nanosheets (pH 14).

SnO_2 nanosheets show the tetragonal lattice parameters a=b= 0.4753 nm, c= 0.3188 nm, with planes 110, 101, and 200 having d-spacings of 0.342 nm, 0.243 nm, and 0.210 nm, respectively.

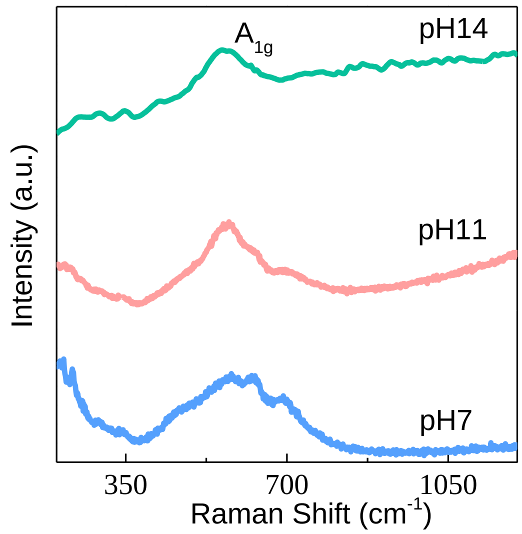

Figure S7: Raman spectra of samples synthesized at different pH conditions.

Table S3: Comparison of specific surface area and pore volume parameters for synthesized SnO_2 nanosheets with literature studies.

Sample	BET Surface Area (m^2/g)	Pore Volume ($cm^3\ g^{-1}$)	References
SnO_2 Nanosheets (pH 7)	236.12	0.108	This work
SnO_2 Nanosheets (pH 11)	124.19	0.046	This work
SnO_2 Nanosheets (pH 14)	64.16	0.025	This work
SnO_2 Nanosheets	62.29	NA	[12]
Nanosheets	21	NA	[13]
Atomically thin nanosheets	173.4	NA	[14]
Crumpled SnO_2 Nanosheets	77.65	0.218	[15]
2D SnO_2	78.21	0.194	[15]
Cone-shaped SnO_2 Nanosheets	180.32	1.028	[16]
SnO_2 Nanosheets	68.78	NA	[3]

NA: Data Not Available

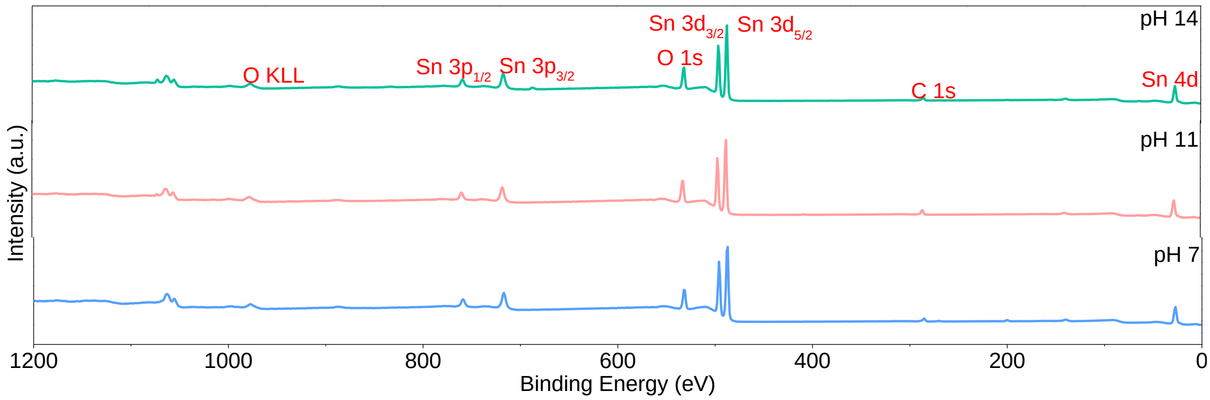

Figure S8: XPS survey spectra of SnO_2 nanosheets synthesized at different pH conditions.

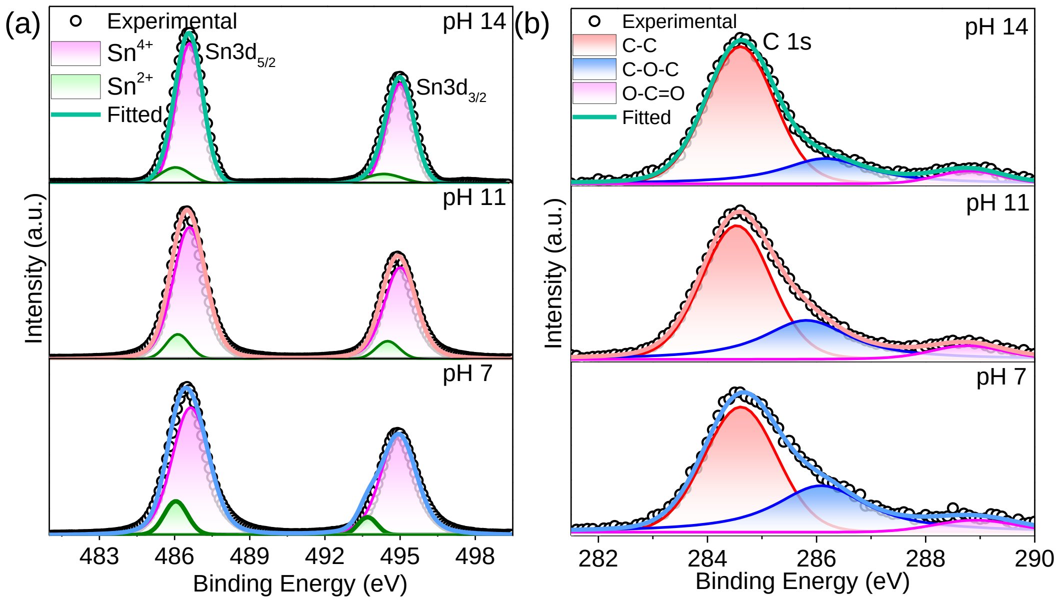

Figure S9: High-resolution Sn3d and C1s XPS spectrum of SnO_2 nanosheets synthesized at different pH conditions. The C1s spectra are carbon-corrected in all cases.

Table S4: High-resolution XPS peak positions of SnO_2 nanosheets synthesized at different pH conditions.

	Sn3d$_{5/2}$			**O1s**			**C1s**			
Peak position (eV)	Sn^{2+}	Sn^{4+}	FWHM (eV)	$O_{lattice}$	$O_{defects}$	O_{chem}	FWHM (eV)	C-C	C-O-C	C=O
pH 14	486.03	486.5	1.32	530.5	531.9	533.1	1.77	284.6	286.2	288.8
pH 11	486.13	486.6	1.56	530.5	531.8	533.0	2.26	284.6	285.8	288.7
pH 7	486.05	486.6	1.71	530.4	531.8	533.0	2.29	284.6	286.0	288.9

Table S5: Oxygen defects concentration of SnO_2 nanosheets synthesized at different pH conditions.

	O-Sn^{4+}		**O-Sn^{2+}**		**O_{Chem}**		**Total O1s**	**Chemisorbed Oxygen ratio**	**Oxygen Defects**
pH	Peak position (eV)	Area under the curve	Peak position (eV)	Area under the curve	Peak position (eV)	Area under the curve	**(%)**		**(%)**
14	530.5	308761	531.9	54107	533.1	42919	52.3	5.5	6.8
11	530.5	128425	531.8	41059	533.0	18618	53.6	5.3	11.7
7	530.4	109967	531.8	30327	533.0	10163	52.3	3.5	10.5

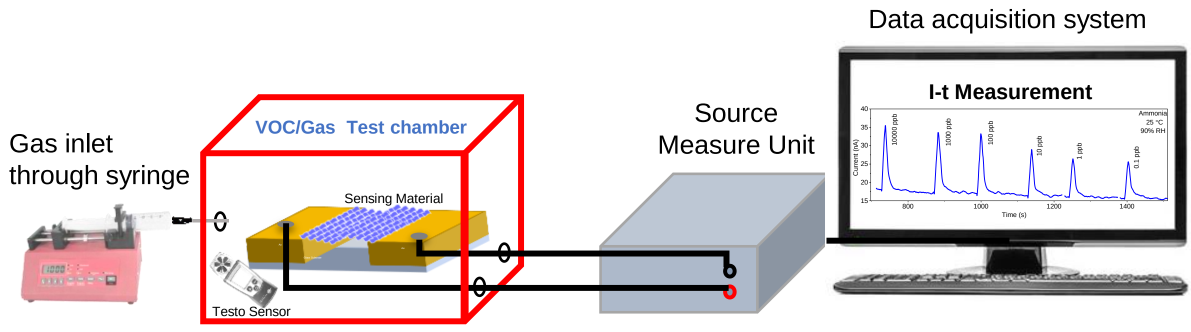

Figure S10: Schematic of the custom gas sensing setup used for dynamic experiments.

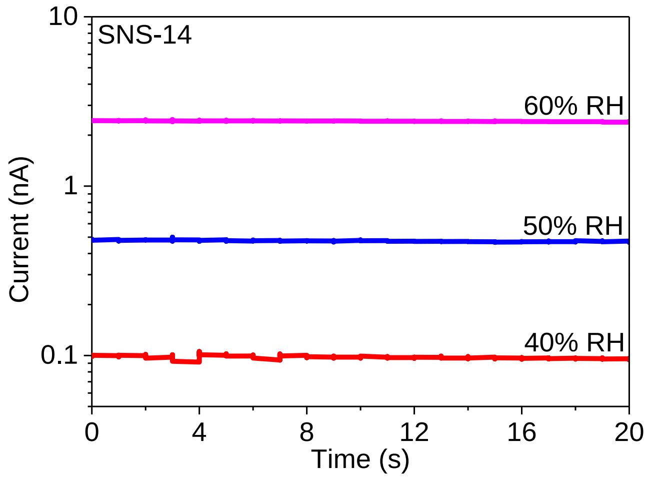

Figure S11: SNS-14 baseline current at varying humidity.

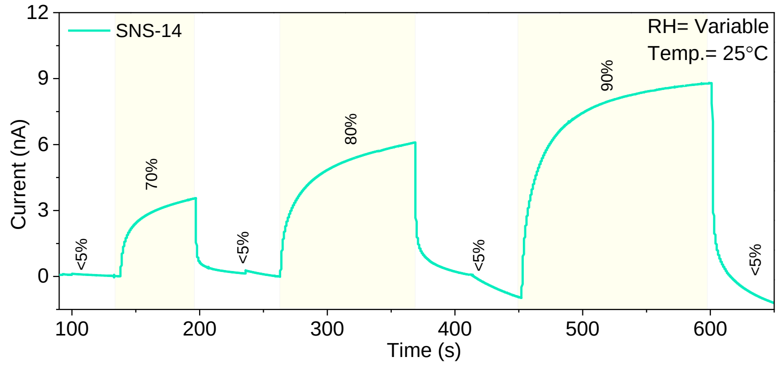

Figure S12: Sensing transients of SNS-14 towards different relative humidity (70-90%RH).

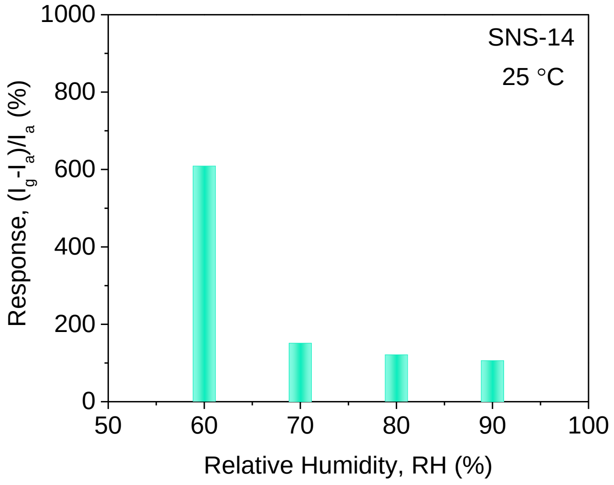

Figure S13: SNS-14 response toward 100 ppm ammonia at a varying relative humidity of 60-90% at room temperature.

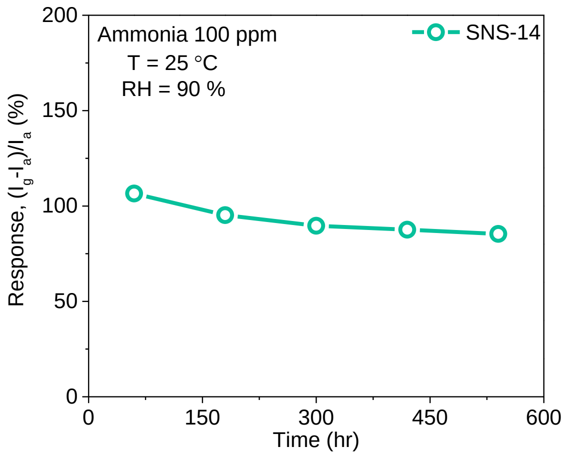

Figure S14: Long-term stability of SNS-14 sensor towards 100 ppm ammonia under humid conditions (90% RH).

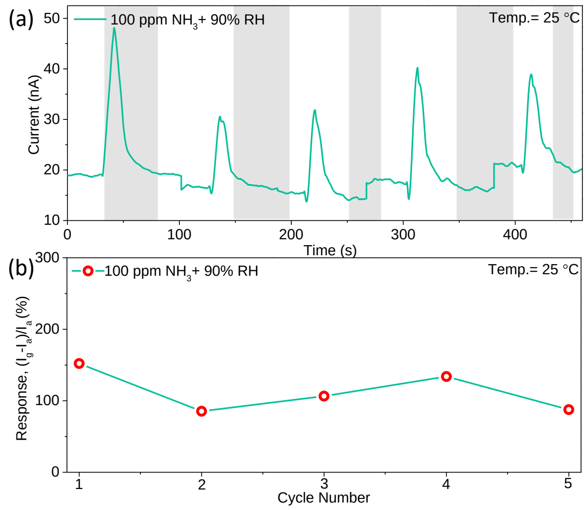

Figure S15: SNS-14 sensor (a) ammonia detecting transients for five cycles and (b) corresponding response value toward 100 ppm NH_3 at 25°C and 90% RH, demonstrating repeatability.

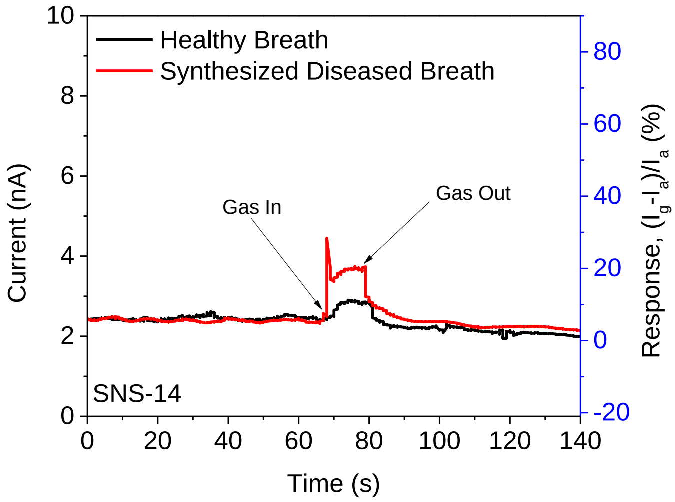

Figure S16: Current response of the SNS-14 toward a healthy person's breath and the simulated diseased breath containing 1 ppm NH_3.

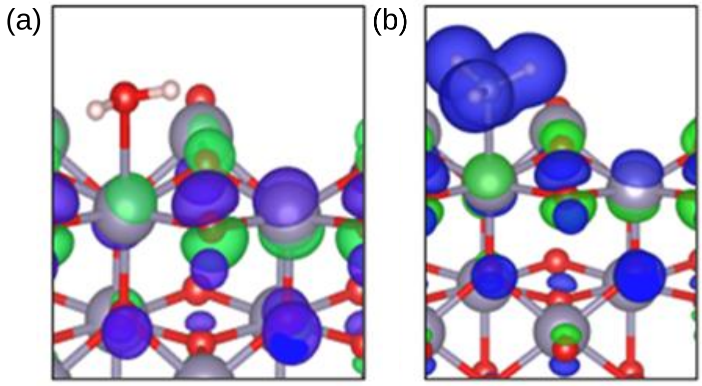

Figure S17: The 3D plots of the charge density difference Δρ(r) of the (a) H_2O and (b) NH_3 molecules on the (110) surface of SnO_2. Electron depletion and accumulation are depicted by blue and green areas, respectively. The isosurfaces are plotted as values of ±0.002 |e| $Å^{-3}$. These depict that the NH_3 molecule donates charge to the surface much more significantly than the H_2O molecule.

References:

(1) Choi, P. G.; Izu, N.; Shirahata, N.; Masuda, Y. Improvement of Sensing Properties for SnO_2 Gas Sensor by Tuning of Exposed Crystal Face. *Sensors Actuators, B Chem.* **2019**, *296* (May), 126655.

(2) Wang, D.; Wan, K.; Zhang, M.; Li, H.; Wang, P.; Wang, X.; Yang, J. Constructing Hierarchical SnO_2 Nanofiber/Nanosheets for Efficient Formaldehyde Detection. *Sensors Actuators, B Chem.* **2019**, *283*, 714–723.

(3) Wan, W.; Li, Y.; Ren, X.; Zhao, Y.; Gao, F.; Zhao, H. 2D SnO_2 Nanosheets: Synthesis, Characterization, Structures, and Excellent Sensing Performance to Ethylene Glycol. *Nanomaterials* **2018**, *8* (2), 112.

(4) Wang, T. T.; Ma, S. Y.; Cheng, L.; Xu, X. L.; Luo, J.; Jiang, X. H.; Li, W. Q.; Jin, W.

X.; Sun, X. X. Performance of 3D SnO_2 Microstructure with Porous Nanosheets for Acetic Acid Sensing. *Mater. Lett.* **2015**, *142*, 141–144.
(5) Zeng, W.; Wu, M.; Li, Y.; Wu, S. Hydrothermal Synthesis of Different SnO_2 Nanosheets with CO Gas Sensing Properties. *J. Mater. Sci. Mater. Electron.* **2013**, *24* (10), 3701–3706.
(6) Zhang, L.; Yin, Y. Hierarchically Mesoporous SnO_2 Nanosheets: Hydrothermal Synthesis and Highly Ethanol-Sensitive Properties Operated at Low Temperature. *Sensors Actuators, B Chem.* **2013**, *185*, 594–601.
(7) Sun, P.; Mei, X.; Cai, Y.; Ma, J.; Sun, Y.; Liang, X.; Liu, F.; Lu, G. Synthesis and Gas Sensing Properties of Hierarchical SnO_2 Nanostructures. *Sensors Actuators, B Chem.* **2013**, *187*, 301–307.
(8) Lou, Z.; Wang, L.; Wang, R.; Fei, T.; Zhang, T. Synthesis and Ethanol Sensing Properties of SnO_2 Nanosheets via a Simple Hydrothermal Route. *Solid. State. Electron.* **2012**, *76*, 91–94.
(9) Sun, P.; Cao, Y.; Liu, J.; Sun, Y.; Ma, J.; Lu, G. Dispersive SnO_2 Nanosheets: Hydrothermal Synthesis and Gas-Sensing Properties. *Sensors Actuators, B Chem.* **2011**, *156* (2), 779–783.
(10) Sun, P.; Zhao, W.; Cao, Y.; Guan, Y.; Sun, Y.; Lu, G. Porous SnO_2 Hierarchical Nanosheets: Hydrothermal Preparation, Growth Mechanism, and Gas Sensing Properties. *CrystEngComm* **2011**, *13* (11), 3718–3724.
(11) Xu, M. H.; Cai, F. S.; Yin, J.; Yuan, Z. H.; Bie, L. J. Facile Synthesis of Highly Ethanol-Sensitive SnO_2 Nanosheets Using Homogeneous Precipitation Method. *Sensors Actuators, B Chem.* **2010**, *145* (2), 875–878.
(12) Xu, R.; Zhang, L. X.; Li, M. W.; Yin, Y. Y.; Yin, J.; Zhu, M. Y.; Chen, J. J.; Wang, Y.; Bie, L. J. Ultrathin SnO_2 Nanosheets with Dominant High-Energy {001} Facets for Low Temperature Formaldehyde Gas Sensor. *Sensors Actuators, B Chem.* **2019**, *289* (August 2018), 186–194.
(13) Wang, H.; Dou, K.; Teoh, W. Y.; Zhan, Y.; Hung, T. F.; Zhang, F.; Xu, J.; Zhang, R.; Rogach, A. L. Engineering of Facets, Band Structure, and Gas-Sensing Properties of Hierarchical Sn^{2+}-Doped SnO_2 Nanostructures. *Adv. Funct. Mater.* **2013**, *23* (38), 4847–4853.
(14) Sun, Y.; Lei, F.; Gao, S.; Pan, B.; Zhou, J.; Xie, Y. Atomically Thin Tin Dioxide Sheets for Efficient Catalytic Oxidation of Carbon Monoxide. *Angew. Chemie - Int. Ed.* **2013**, *52* (40), 10569–10572.
(15) Kim, R.; Jang, J. S.; Kim, D. H.; Kang, J. Y.; Cho, H. J.; Jeong, Y. J.; Kim, I. D. A General Synthesis of Crumpled Metal Oxide Nanosheets as Superior Chemiresistive Sensing Layers. *Adv. Funct. Mater.* **2019**, *29* (31), 1–10.
(16) Wang, C.; Zhou, Y.; Ge, M.; Xu, X.; Zhang, Z.; Jiang, J. Z. Large-Scale Synthesis of SnO_2 Nanosheets with High Lithium Storage Capacity. *J. Am. Chem. Soc.* **2010**, *132* (1), 46–47.